Hindawi
Shock and Vibration
Volume 2020, Article ID 8825505, 9 pages
https://doi.org/10.1155/2020/8825505

*Research Article*

# Discussions on the Complete Strain Energy Characteristics of Deep Granite and Assessment of Rockburst Tendency

**Lu Chen and Lijie Guo**

*Beijing General Research Institute of Mining and Metallurgy, Beijing 102628, China*

Correspondence should be addressed to Lijie Guo; guolijie@bgrimm.com

Received 20 March 2020; Revised 15 June 2020; Accepted 10 July 2020; Published 26 July 2020

Academic Editor: Hongwei Yang



In deep mining, the rockburst hazard has become a prominent problem. Rockburst is difficult to be predicted, and it gives a severe threat to mining safety. In this paper, the triaxial compressive tests with an acoustic emission (AE) device and full cyclic loading and unloading tests were carried out, respectively, to present characteristics of linear elastic strain energy and peak strain energy. Also, to consider the time-delay strain characteristics of granite found in the abovementioned tests, a new stage loading and unloading test with dual monitoring systems was designed and performed. Through 20 days' time-delay strain monitoring, the peak-strength strain energy was further modified. The results showed that the peak strain energy is approximate 1.2-1.3 times than linear elastic strain energy under the same confining pressure, and after considering the time-delay strain effect, the modified maximal strain energy value of the deep granite significantly increased. The peak strain energy values are further enhanced from $1.0 \times 10^4$ J/m$^3$ to $1.8 \times 10^4$ J/m$^3$, respectively. At last, by taking advantage of the strain energy index model of rockburst, the tendency and intensity of rockburst were assessed contrastively.

## 1. Introduction

With the depletion of shallow resources, deep mining is an inevitable trend of future mining work. Nowadays, the deepest mine in the world (Mponeng Gold Mine in South Africa) has exceeded 4000 m, and some scholars predicted that the mining extends at a rate of 10–25 m per year in depth. In the next 10 to 15 years, more than 50% iron ore mines will be over 1000 m deep in China [1]. In deep mining, due to the complex geological environment with high geostress, high pore water pressure, and high rock temperature, the rockburst hazard is becoming a prominent problem during the deep mining process. Also, as the mining depth increases, the rockburst will occur more frequently and intensively. The rockburst is defined as a sudden or violent damage during the host rock excavation [2]. Rockburst hazard is a long-standing problem and serious threat to mine safety, so many scholars try to predict rockburst employing various methods. Kornowski and Kurzeja [3] built an expert system of hazard evaluation to predict rockburst probability. Hosseini [4] used the passive seismic velocity tomography and image subtraction technique to estimate the rockburst potential. Li et al. [5] adopted the microseismic monitoring data to analyze the frequent rockbursts. Faradonbeh and Taheri [6] used the three mining techniques to predict the rockburst hazard in deep underground. Faradonbeh et al. [7] studied the rockburst clustering problem by application of self-organizing map and fuzzy c-mean techniques. Ghasemi et al. [8] evaluated the rockburst occurrence and intensity with a decision tree approach. Rockburst is an extremely complex rock failure process, and many factors can affect the occurrence of rockburst disaster. Jiang et al. [9] proposed a combined early warning method, including the microseismic monitoring data, the electromagnetic emission monitoring data, and the drilling cutting data, to predict the rockburst. Jia et al. [10] used the optimized unascertained measure theory to build a comprehensive prediction model of rockburst tendency.

Although numerous researches have been conducted, because of the complicated process and multiple influencing factors, rockburst problem is not well solved and still a hot topic in rock mechanics and mining engineering. Also, it is hard to obtain accurate data to assess the rockburst mechanism and process from the unitary in situ monitoring activities. So, scholars designed and carried out extensive laboratory experiments to simulate the rockburst process or explore the rockburst mechanism, such as the bedding plane influence test [11], true-triaxial test [12, 13], size effect test [14], and loading and unloading test [15], to name a few. A large number of studies show that it is more scientific and effective for energy theory to analyze the rockburst problem [16–18]. Under the framework of the rock energy theory system, a large number of rock mass violent failures or rockburst problems have been studied. Khademian and Ozbay [19] researched the violent rock failures model in tunneling and shaft boring based on energy balance calculations. As the research continues, the whole energy process of rockburst is gradually refined, and the main considering energy during rock failure process is the initial elastic strain energy. Weng et al. [20] studied the rockburst characteristics using a strain energy density index in the numerical simulation process; using a strain energy density index in the numerical simulation process, Shou et al. [21] built a critical condition of the zonal disintegration in deep rock masses based on the strain energy density approach; Razavi et al. [22] obtained a mixed mode fracture load of granite rock with application of an average strain energy density criterion. Also, scholars studied other energy components, such as redistributed energy induced by mining or excavation [23–25], dissipative energy during rock failure [26, 27], and released energy accompanied by rockburst [28, 29]. Among these energy analysis models, the elastic strain energy stored in rock mass is the origin of all energy process, and it is also the main power source of rockburst disaster. As described in the abovementioned references' review, the existing researches mainly focus on linear elastic strain storage energy, and its value can be obtained by combining the AE monitoring test [30–32]. However, the linear elastic storage energy ignores the part of strain energy that is below the peak strength and above the elastic-plastic boundary point. In this part, although the rock has been damaged gradually, it still has a certain strain energy storage capacity.

In this paper, to discuss the complete strain energy characteristics of deep granite, firstly, the triaxial loading tests accompanied with an AE monitoring system of deep granite were carried out. The initial crack point of rocks could be visually obtained corresponding with AE data. Then, the linear elastic strain energy value could be calculated by the elastic modulus and stress value at the initial crack point. Secondly, to study the capacity of peak-strength strain energy storage of deep granite, a series of cyclic loading and unloading tests under typical confining pressures was carried out. After analyzing the elasticity modulus of peak unloading curve and peak stress, the peak-strength strain energy could also be presented. Thirdly, based on the time-delay strain characteristics of rock found in full loading and unloading tests, a novel step loading and unloading test was designed and performed. Through time-delay strain monitoring, the peak-strength strain energy could be further modified. At last, using the values of strain energy and employing the typical rockburst prediction model, the tendency and intensity of rockburst were assessed contrastively.

## 2. Linear Elastic Strain Energy Confirmed by AE Monitoring

*2.1. Granite Samples and Basic Parameters.* In the tests, the rock specimen is granite, drilled from -895 level of Sanshandao Gold Mine (Shandong Province, China), with the mineral composition of quartz, anorthose, biotite, and alkali feldspar. The density of rock samples is 2.72 g/cm$^3$, and the porosity is 0.59%. To make sure of the uniformity, all the rock samples were cut form a whole block rockmass without any obvious cracks. According to the proposed approach of ISRM, the allowed deviation of roughness at the two ends for the specimen is ±0.05 mm, and the allowed perpendicularity deviation is ±0.25°. In the tests, 25 standard rock samples with 50 mm diameter and 100 mm height were obtained, as shown in Figure 1.

*2.2. Triaxial Compressive Test with AE Monitoring.* During the tests, the TAW-2000 microcomputer servo rock testing machine was adopted to carry out the granite triaxial compressive tests, and the SAEU2S digital AE instrument was used for AE monitoring. During the test, with the increasing loading, the rock samples would undergo crack closure, crack initial, crack connection, and peak stage. At each special point, there would be an obvious change of AE events, so the initial crack point of granite could be found by the AE monitoring data. The test devices are shown in Figure 2.

After 15 tests with different confining pressures (5 MPa, 10 MPa, 20 MPa, 30 MPa, and 40 MPa), the stress-strain curves with AE data from triaxial compressive tests were obtained, to display the part of AE events corresponding to the initial crack point, and to eliminate the display problem caused by overlarge AE events at the peak stage, the detailed diagram of AE events should be presented. The typical testing curves and their partial detailed diagram are shown in Figure 3.

As shown in Figure 3, for calculation of linear elastic strain energy of deep granite, the initial crack point of granite acquired acoustic emission monitoring was recognized as the turning point of rock from strain energy storage to energy dissipation.

*2.3. Result of Linear Elastic Strain Energy.* After analysis of 15 stress-strain curves with AE monitoring data, the elastic modulus and stress value at the initial crack point are confirmed to calculate linear elastic strain energy.

$$W_e = \frac{1}{2} E \sigma_{ci}^2, \tag{1}$$

where $W_e$ is the linear elastic strain energy, $E$ is the elastic modulus, and $\sigma_{ci}$ is the value of initial crack stress.

Figure 1: The granite samples and their optical image.

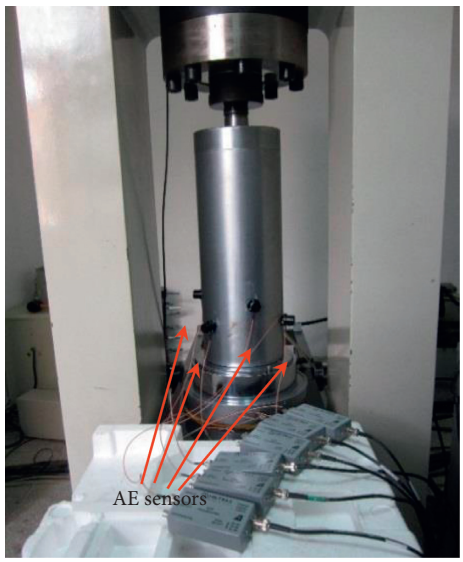


Figure 2: Triaxial compressive test of granite with AE monitoring.

Table 1 shows the initial crack stress, the elastic modulus, and Poisson's ratio corresponding to the initial crack point and the calculated linear elastic strain energy density of deep granite with 5 typical confining pressures. Based on the test data in Table 1, the linear elastic strain energy density curves of deep granite under different confining pressures can be fitted, as shown in Figure 4.

As shown in Figure 4, with increase of confining pressure, the linear elastic strain energy density value presents a linear growth law. When the confining pressure is 40 MPa, the linear elastic strain energy density value of granite is close to $1.4e^5$ J/m$^3$.

## 3. Peak Strain Energy Confirmed by the Full Cyclic Loading and Unloading Test

In order to supplement the elastic strain energy storage capacity of granite in the stage after the initial crack point and before the peak strength, the elastic stress-strain curve of this stage needs to be acquired. However, after the initial crack point, the elastic deformation and plastic damage deformation under the loading path are mixed together and cannot be distinguished. If the unloading test is carried out at this stage, since the elastic strain can recover, while the plastic strain cannot recover, the unloading curve can present the loading elastic stress-strain curve. Based on this view, the full cyclic loading and unloading tests are conducted to research the peak strain energy of deep granite.

*3.1. Full Cyclic Loading and Unloading Tests.* In the tests, the instrument is a MTS815 rock testing machine. In the full cyclic loading and unloading tests on granite samples, also 5 groups of typical confining pressure (5 MPa, 10 MPa, 20 MPa, 30 MPa, and 40 MPa) were selected. Based on the peak-strength values obtained from triaxial compressive tests, to select a suitable initial value for the cyclic loading and avoid the effect of fatigue damage caused by multiple cycles, the number of loading and unloading cycles should be controlled strictly. After the preliminary testing, the first cyclic point was set at 150 MPa of the axial pressure level and cycled at every 50 MPa. When the stress-strain curve seemingly approached the peak strength of the triaxial compressive test under the same confining pressure, the cyclic step was set at every 5 MPa, and after the peak strength, the cyclic space was readjusted to every 50 MPa. The loading and unloading path diagrams are shown in Figure 5.

*3.2. Testing Result and Peak Strain Energy Analysis.* After the full cyclic loading and unloading testing, the full cyclic stress-strain curves of 5 groups of granite samples under different confining pressure were obtained, and the specific data of peak unloading curves were also determined. The typical testing data curves are shown in Figure 6.

As shown in Figure 6, it is easy to confirm the peak stress. To obtain the unloading elastic modulus value for calculating the peak strain energy, the unloading curve at the peak-strength point was selected. Because the unloading curve is not a straight line, the slope value of the tangent line at the peak-strength point (red line with arrow) was recognized as the unloading elastic modulus. According to the peak unloading curve data, the curve between confining pressure and peak strain energy density can be fitted in the same way as energy density. The comparing data with the linear elastic strain energy diagram are shown in Figure 7.

As shown in Figure 7, with the increase in confining pressure, the strain energy density obtained by these two methods presents the linear growth law. Also, the peak strain energy is about 1.2 times than the linear elastic strain energy under the same confining pressure.

## 4. Maximum Strain Energy Considering Time-Delay Strain Characteristics

*4.1. Time-Delay Strain Characteristics of Deep Granite.* In the abovementioned full cyclic loading and unloading studies, it is found that although the rock samples are in the linear elastic stage, there is still a certain difference between the loading curve and the unloading curve. Because there is no plastic effect, this strain difference must be the recoverable elastic strain and may recover in the next period of time. In view of this finding, 20% and 40% peak stress unloading tests were performed to verify the time-delay strain characteristic of granite. The testing curves with 10 MPa and 20 MPa confining pressure are shown in Figure 8.

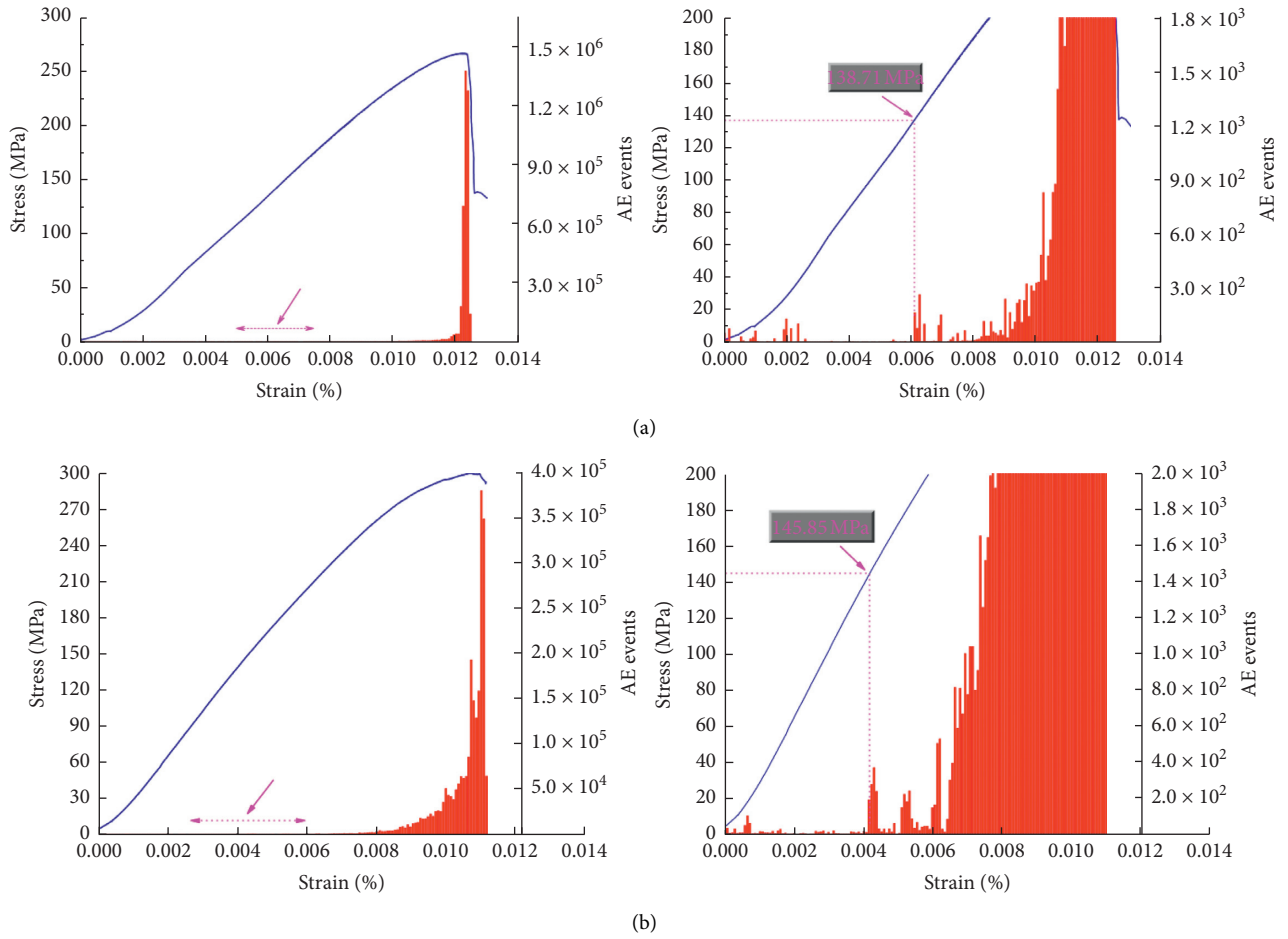


Figure 3: Typical stress-strain curve with AE events and its partial diagram of an initial crack point. (a) No. 1 testing specimen with 20 MPa confining pressure. (b) No. 2 testing specimen with 20 MPa confining pressure.

Table 1: The testing data and linear elastic strain energy.

| Confining pressure (MPa) | Elasticity modulus (GPa) | Poisson's ratio | Initial crack stress (MPa) | Strain energy density (J·m$^3$) |
|---|---|---|---|---|
| 5.0 | 60.30 | 0.21 | 93.50 | $7.16E+04$ |
| 5.0 | 59.97 | 0.19 | 95.71 | $6.78E+04$ |
| 5.0 | 61.16 | 0.21 | 110.47 | $7.07E+04$ |
| 10.0 | 76.13 | 0.21 | 128.02 | $7.82E+04$ |
| 10.0 | 74.56 | 0.23 | 137.19 | $8.83E+04$ |
| 10.0 | 79.92 | 0.20 | 128.48 | $7.89E+04$ |
| 20.0 | 85.27 | 0.23 | 138.71 | $9.35E+04$ |
| 20.0 | 82.76 | 0.22 | 145.85 | $1.03E+05$ |
| 20.0 | 78.01 | 0.23 | 164.03 | $9.10E+04$ |
| 30.0 | 80.94 | 0.21 | 174.23 | $1.26E+05$ |
| 30.0 | 91.86 | 0.23 | 194.00 | $1.12E+05$ |
| 30.0 | 87.12 | 0.22 | 208.83 | $1.19E+05$ |
| 40.0 | 86.24 | 0.24 | 214.94 | $1.20E+05$ |
| 40.0 | 87.60 | 0.22 | 191.46 | $1.34E+05$ |
| 40.0 | 83.90 | 0.23 | 249.61 | $1.39E+05$ |

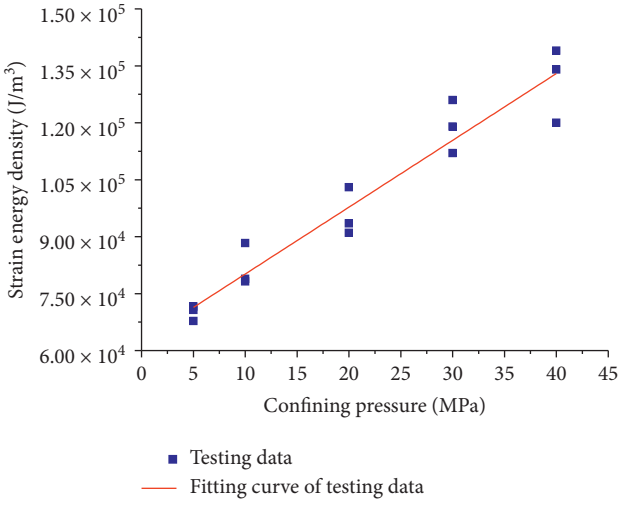


Figure 4: Linear elastic strain energy by the triaxial compressive test.

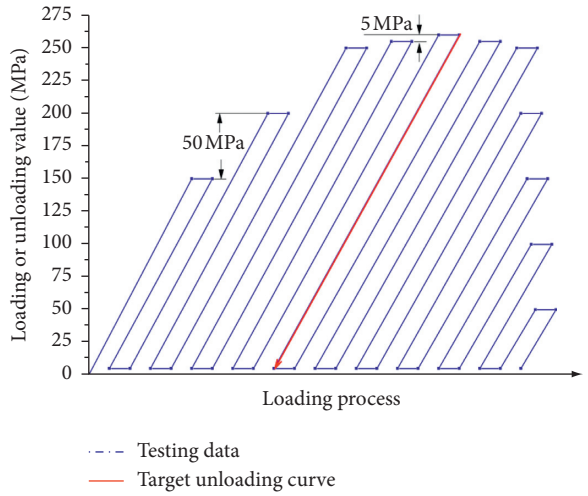


Figure 5: The loading and unloading path diagram.

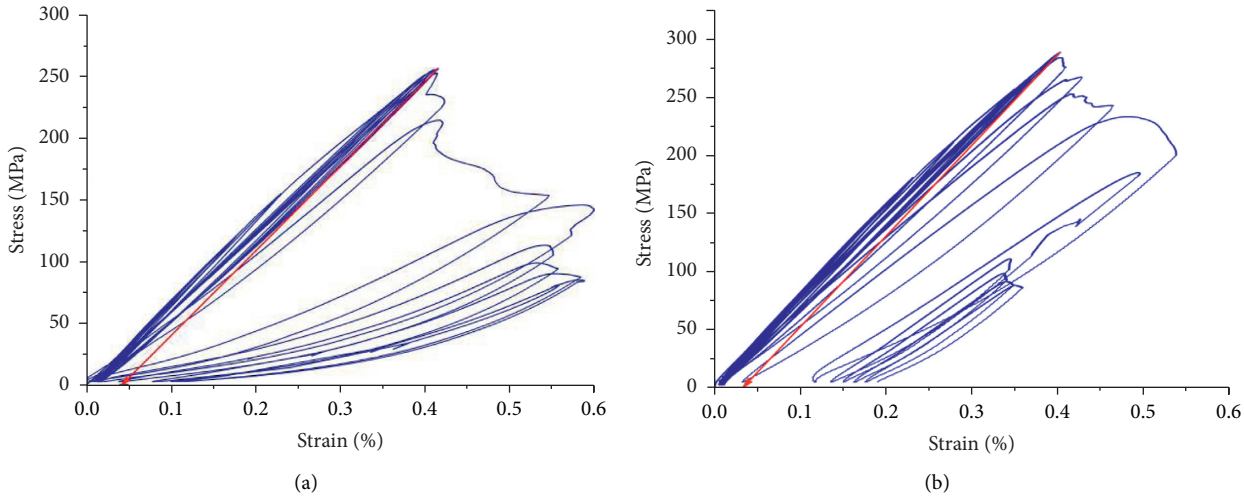


Figure 6: Typical stress-strain loading and unloading curves of granite. (a) 20 MPa. (b) 30 MPa.

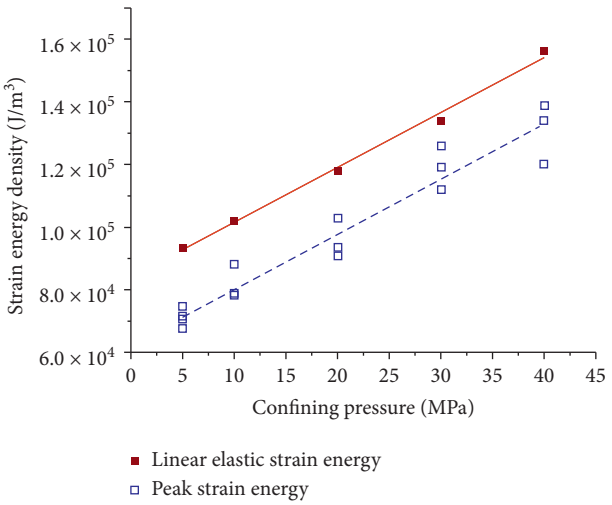


Figure 7: Strain energy density values of the peak unloading and crack initiation point method.

As shown in Figure 8, whether the loading is 20% or 40% peak stress, after 5 times loading and unloading, each unloading curve exactly coincides with the previous one. This also proves that a limited number of cycles do not cause fatigue damage. But, there is an obvious strain distance between the first loading curve and other curves, and the distance values are 0.01381 and 0.01577 corresponding to 20% and 40% peak stress under 10 MPa confining pressure. Under the 20 MPa confining pressure, the values are 0.01543 and 0.01846, respectively. From these strain distance values, two main conclusions can be reflected. Firstly, there is an obvious time-delay characteristic for the deep granite. Secondly, the time-delay strain mostly occurs in the early loading process (for 0.01577–0.01381 = 0.00196, it is about 88% time-delay strain occurred in the previous 20% peak stress, and only 12% time-delay strain occurred in the next 20% peak stress under 10 MPa confining pressure. Also, the values are 84% and 16% for the time-delay strain occurred in the previous 20% and the next 20% peak stress under 20 MPa confining pressure).

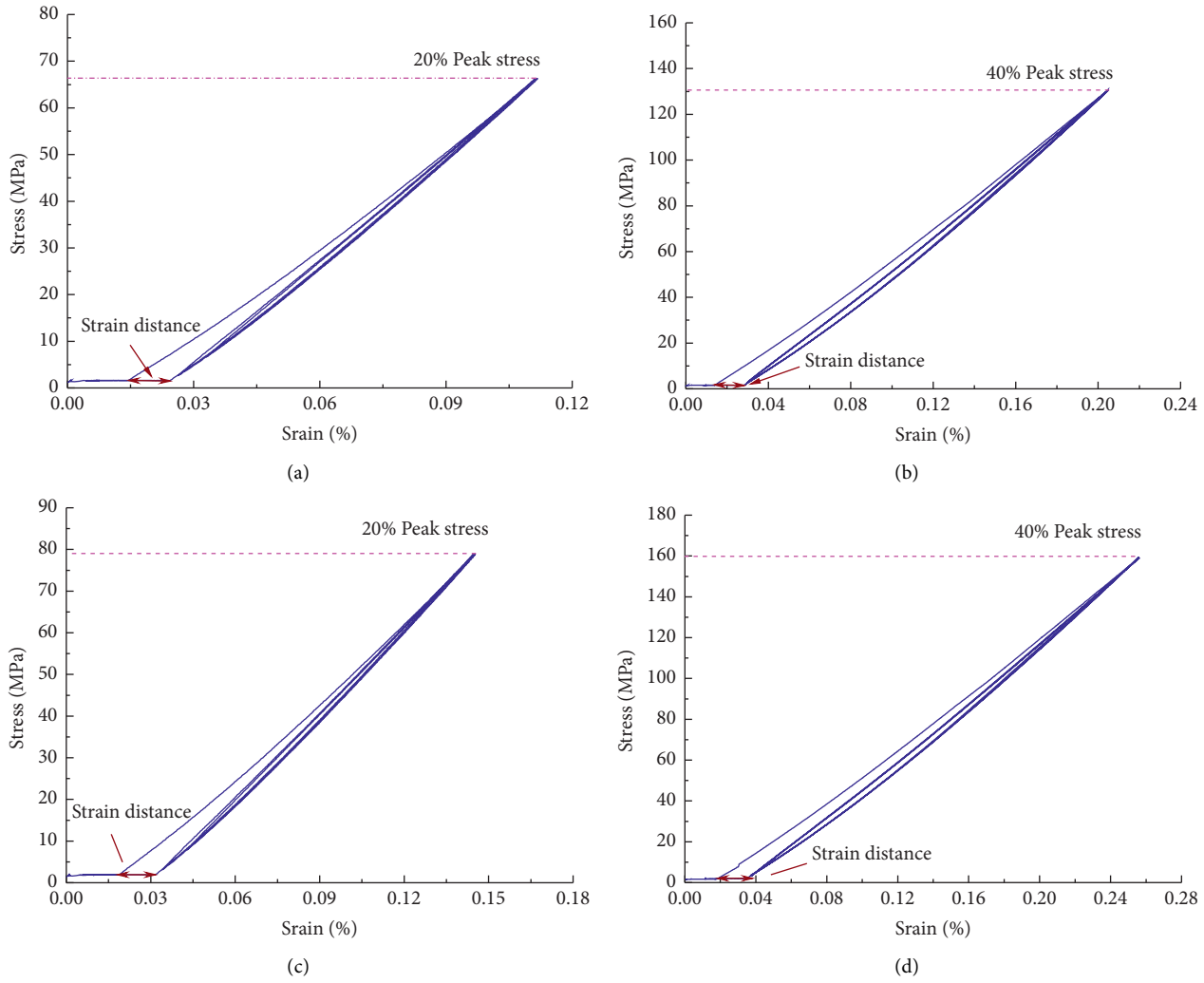


Figure 8: Time-delay characteristic verification test of granite. (a) 20% peak stress under 10 MPa. (b) 40% peak stress under 10 MPa. (c) 20% peak stress under 20 MPa. (d) 40% peak stress under 20 MPa.

*4.2. Stage Cyclic Loading and Unloading Test with Dual Monitoring Systems.* In order to quantify the time-delay strain characteristics of deep granite more accurately, stage cyclic loading and unloading tests with dual monitoring systems (extensometer system and strain rosette) were carried out. The dual monitoring systems are shown in Figure 9.

To obtain the most comprehensive time-delay strain value and ensure the rock sample does not develop obvious macroscopic cracks which can affect the next strain rebound monitoring, the largest loading value is set as the long-term strength of deep granite. After 3 groups of testing, the typical stage loading and unloading testing curves are as shown in Figure 10.

As shown in Figure 10, after the stage loading and unloading test, the axial and lateral strain both have the certain noninstantaneous rebound strain. In order to acquire the noninstantaneous rebound strain value and confirm the

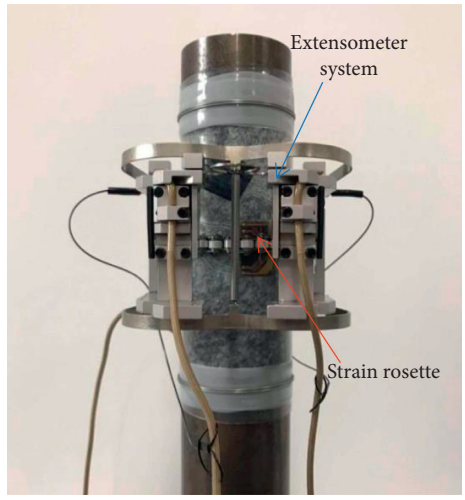


Figure 9: Extensometer and the strain monitoring system during the test.

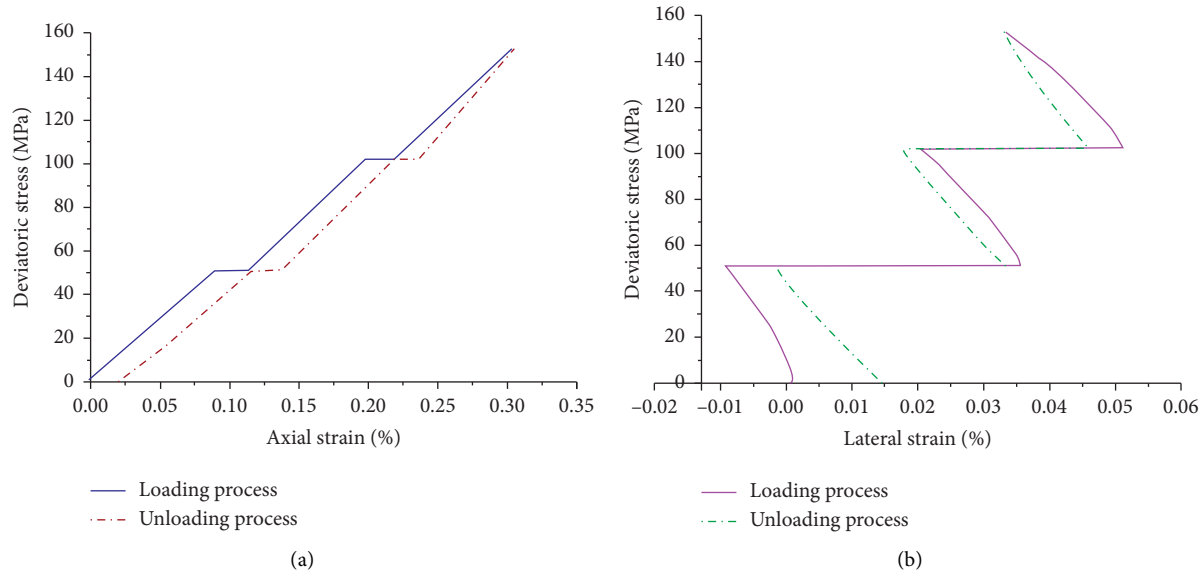


Figure 10: Typical stage loading and unloading testing curve. (a) Axial time-delay strain. (b) Lateral time-delay strain.

time of strain recovery, the prepasted strain gauges on the granite sample were connected to the strain collector and put into the incubator to eliminate the influence of temperature on the strain. The strain rebound value was collected for 2 hours every day with a sampling interval of 5 minutes. After 20 days of continuous monitoring, the monitoring data are as shown in Figure 11.

As shown in Figure 11, the axial strain rebound microstrain value is 132, and the lateral strain rebound microstrain value is 82, accounting for 5.6% and 22.7% of the corresponding total strain, respectively. Hence, for the maximal strain energy of deep granite, the value should consider the extra 5.6% addition in the vertical direction and 22.7% in the lateral direction.

*4.3. Rockburst Tendency Prediction Based on Strain Energy.* In rockburst tendency analysis, the elastic strain energy model is often taken as the index. According to the elastic strain energy model, rockburst intensity can be divided into four grades:

$$W_e < 40\,\text{kJ/m}^3, \quad \text{I: Weak}, \tag{2}$$

$$40\,\text{kJ/m}^3 \le W_e < 100\,\text{kJ/m}^3, \quad \text{II: Medium}, \tag{3}$$

$$100\,\text{kJ/m}^3 \le W_e < 200\,\text{kJ/m}^3, \quad \text{III: Strong}, \tag{4}$$

$$200\,\text{kJ/m}^3 < W_e, \quad \text{IV: Intensity}. \tag{5}$$

The abovementioned research introduced different methods to obtain the strain energy of deep granite and calculated the corresponding strain energy density. Here, based on the calculated strain energy values, the rockburst strength grades are provided, the results are shown in Table 2, and the fitted curve are shown in Figure 12.

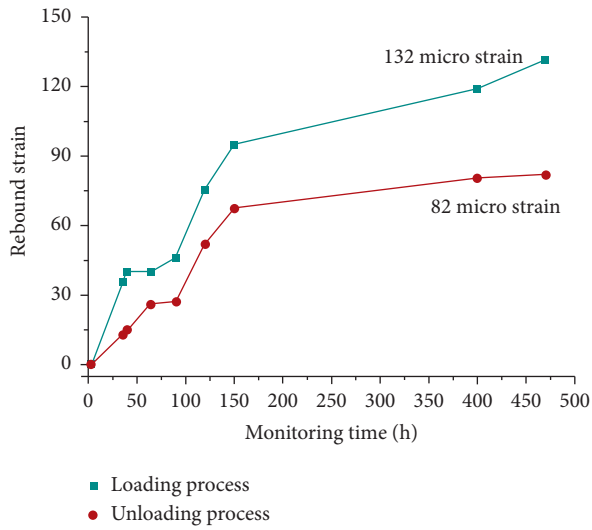


Figure 11: Elastic time-delay strain rebound monitoring data.

From Table 2 and Figure 12, it is easily found that the rockburst grades present an obvious increasing trend after considering the peak strain energy and time-delay strain energy. When the testing granite were located in a lower geostress condition (less than 20 MPa), the rockburst grades present as the "Weak" with the linear strain energy approach, and the rockburst grades will improve to the "medium" using the maximal strain energy approach. Also, even under the 40 MPa confining pressure, the strain energy density is increased by $4.3e^4\,\text{J/m}^3$. Therefore, scientifically measuring the strain energy storage capacity of deep granite can provide accurate data support for defining the magnitude of rockburst and other dynamic disasters.

Table 2: Rockburst tendency under different confining pressures.

| Confining pressure (MPa) | Linear strain energy density | Rockburst grades | Peak strain energy density | Rockburst grades | Maximal strain energy density | Rockburst grades |
|---|---|---|---|---|---|---|
| 5 | $7.0E+04$ | Weak | $9.31E+04$ | Weak | $1.04E+05$ | Medium |
| 10 | $8.2E+04$ | Weak | $1.02E+05$ | Medium | $1.14E+05$ | Medium |
| 20 | $9.6E+04$ | Weak | $1.18E+05$ | Medium | $1.32E+05$ | Medium |
| 30 | $1.2E+05$ | Medium | $1.34E+05$ | Medium | $1.49E+05$ | Medium |
| 40 | $1.31E+05$ | Medium | $1.56E+05$ | Medium | $1.74E+05$ | Medium |

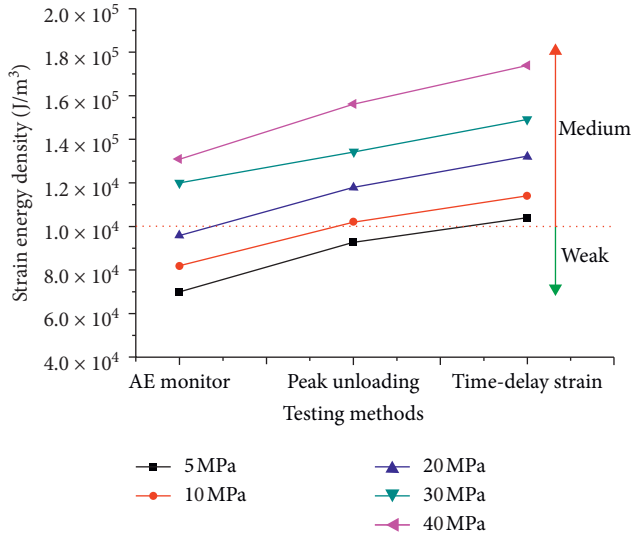


Figure 12: Strain energy and rockburst tendency analysis.

## 5. Conclusions

In this article, three different testing methods were adopted to present the storage capacity of strain energy, and the main conclusions are as follows:

(1) In this study, based on the AE monitoring data, the initial stress point under different confining pressures were confirmed, and the linear elastic strain energy of deep granite was calculated. The testing results showed that, with the increase in confining pressure, the linear elastic strain energy density value presents a linear growth law. Also, when the confining pressure is 40 MPa, the linear elastic strain energy density value of granite is close to $1.4e^5$ J/m$^3$.

(2) To supplement the elastic strain energy storage capacity of granite in the stage after the initial crack point and before the peak strength, the full cyclic loading and unloading tests are designed and carried out to assess the peak strain energy. After testing, the peak strain energy also presents the linear growth law. Also, the peak strain energy is about 1.2 times than linear elastic strain energy under the same confining pressure.

(3) During the full cyclic loading and unloading studies, the deep granite presents obvious time-delay characteristics, so the 20% and 40% peak stress unloading tests were performed to testify the time-delay characteristics. The stage loading and unloading tests with a dual monitoring system were carried out to acquire time-delay value and recovery time. The testing data indicated that there are 132 microstrains in the axial direction, and the 82 microstrains in the lateral direction can recover in 20 days.

(4) At last, the rockburst tendency was analyzed by employing the elastic strain energy index model. After investigating, it is easily found that the rockburst grades present an obvious increasing trend after considering the peak strain energy and time-delay strain energy. Under the 40 MPa confining pressure, the strain energy density is increased by $4.3e^4$ J/m$^3$. A precise strain energy characterization method can provide accurate data support for rockburst evaluation.

## Data Availability

All data used to support the findings of this study are available from the corresponding author upon request.

## Conflicts of Interest

All the authors declare that there are no conflicts of interest regarding the publication of this paper.

## Acknowledgments

The authors acknowledge the financial supports from the State Key Research Development Program of China (No. 2018YFE0123000).

## References

[1] H. Xie, H. Konietzky, and H. W. Zhou, "Special issue "deep mining"," *Rock Mechanics and Rock Engineering*, vol. 52, no. 5, pp. 1415-1416, 2019.

[2] P. K. Kaiser, D. D. Tannant, and D. R. McCreath, *Canadian Rockburst Support Handbook*, Geomechanics Research Centre/Laurentian University, Sudbury, Canada, 1996.

[3] J. Kornowski and J. Kurzeja, "Prediction of rockburst probability given seismic energy and factors definedby the expert method of hazard evaluation (MRG)," *Acta Geophysica*, vol. 60, no. 2, pp. 472–486, 2012.

[4] N. Hosseini, "Evaluation of the rockburst potential in longwall coal mining using passive seismic velocity tomography and image subtraction technique," *Journal of Seismology*, vol. 21, no. 5, pp. 1101–1110, 2017.

[5] Z.-L. Li, X.-Q. He, L.-M. Dou, and G.-F. Wang, "Rockburst occurrences and microseismicity in a longwall panel experiencing frequent rockbursts," *Geosciences Journal*, vol. 22, no. 4, pp. 623–639, 2018.

[6] R. S. Faradonbeh and A. Taheri, "Long-term prediction of rockburst hazard in deep underground openings using three robust data mining techniques," *Engineering with Computers*, vol. 35, no. 2, pp. 659–675, 2019.

[7] R. S. Faradonbeh, S. S. Haghshenas, A. Taheri, and R. Mikaeil, "Application of self-organizing map and fuzzy c-mean techniques for rockburst clustering in deep underground projects," *Neural Computing and Applications*, vol. 32, no. 12, pp. 8545–8559, 2019.

[8] E. Ghasemi, H. Gholizadeh, and A. C. Adoko, "Evaluation of rockburst occurrence and intensity in underground structures using decision tree approach," *Engineering with Computers*, vol. 36, no. 1, pp. 213–225, 2020.

[9] B. Y. Jiang, L. G. Wang, Y. L. Lu, C. Q. Wang, and D. Ma, "Combined early warning method for rockburst in a Deep Island, fully mechanized caving face," *Arabian Journal of Geosciences*, vol. 9, no. 20, p. 743, 2016.

[10] Q. J. Jia, L. Wu, B. Li, C. H. Chen, and Y. X. Peng, "The comprehensive prediction model of rockburst tendency in tunnel based on optimized unascertained measure theory," *Geotechnical and Geological Engineering*, vol. 37, no. 4, pp. 3399–3411, 2019.

[11] M. C. He, W. Nie, Z. Y. Zhao, and W. Guo, "Experimental investigation of bedding plane orientation on the rockburst behavior of sandstone," *Rock Mechanics and Rock Engineering*, vol. 45, no. 3, pp. 311–326, 2012.

[12] K. Du, M. Tao, X.-B. Li, and J. Zhou, "Experimental study of slabbing and rockburst induced by true-triaxial unloading and local dynamic disturbance," *Rock Mechanics and Rock Engineering*, vol. 49, no. 9, pp. 3437–3453, 2016.

[13] G. S. Su, X. T. Feng, J. H. Wang, J. Q. Jiang, and L. H. Hu, "Experimental study of remotely triggered rockburst induced by a tunnel axial dynamic disturbance under true-triaxial conditions," *Rock Mechanics and Rock Engineering*, vol. 50, no. 8, pp. 2207–2226, 2017.

[14] F. Zhao and M. C. He, "Size effects on granite behavior under unloading rockburst test," *Bulletin of Engineering Geology and the Environment*, vol. 76, no. 3, pp. 1183–1197, 2017.

[15] F.-Q. Gong, C. Wu, S. Luo, and J.-Y. Yan, "Load–unload response ratio characteristics of rock materials and their application in prediction of rockburst proneness," *Bulletin of Engineering Geology and the Environment*, vol. 78, no. 7, pp. 5445–5466, 2019.

[16] G. N. Feit, O. N. Malinnikova, V. S. Zykov, and V. A. Rudakov, "Prediction of rockburst and sudden outburst hazard on the basis of estimate of rock-mass energy," *Journal of Mining Science*, vol. 38, no. 1, pp. 61–63, 2002.

[17] D. Y. Li, Z. Sun, T. Xie, X. B. Li, and P. G. Ranjith, "Energy evolution characteristics of hard rock during triaxial failure with different loading and unloading paths," *Engineering Geology*, vol. 228, pp. 270–281, 2017.

[18] J. Xu, J. D. Jiang, N. Xu, Q. S. Liu, and Y. F. Gao, "A new energy index for evaluating the tendency of rockburst and its engineering application," *Engineering Geology*, vol. 230, pp. 46–54, 2017.

[19] Z. Khademian and U. Ozbay, "Modeling violent rock failures in tunneling and shaft boring based on energy balance calculations," *Tunnelling and Underground Space Technology*, vol. 90, pp. 62–75, 2019.

[20] L. Weng, L. Q. Huang, A. Taheri, and X. B. Li, "Rockburst characteristics and numerical simulation based on a strain energy density index: a case study of a roadway in Linglong gold mine, China," *Tunnelling and Underground Space Technology*, vol. 69, pp. 223–232, 2017.

[21] Y. D. Shou, X. P. Zhou, and Q. H. Qian, "A critical condition of the zonal disintegration in deep rock masses: strain energy density approach," *Theoretical and Applied Fracture Mechanics*, vol. 97, pp. 322–332, 2018.

[22] S. M. J. Razavi, M. R. M. Aliha, and F. Berto, "Application of an average strain energy density criterion to obtain the mixed mode fracture load of granite rock tested with the cracked asymmetric four-point bend specimens," *Theoretical and Applied Fracture Mechanics*, vol. 97, pp. 419–425, 2018.

[23] X. J. Dong, A. Karrech, H. Basarir, M. Elchalakani, and C. C. Qi, "Analytical solution of energy redistribution in rectangular openings upon insitu rock mass alteration," *International Journal of Rock Mechanics and Mining Sciences*, vol. 106, pp. 74–83, 2018.

[24] M. Sepehri, D. B. Apel, S. Adeeb, P. Leveille, and R. A. Hall, "Evaluation of mining-induced energy and rockburst prediction at a diamond mine in Canada using a full 3D elastoplastic finite element model," *Engineering Geology*, vol. 266, Article ID 105457, 2020.

[25] G. F. Wang, S. Y. Gong, L. M. Dou, H. Wang, W. Cai, and A. Y. Cao, "Rockburst characteristics in syncline regions and microseismic precursors based on energy density clouds," *Tunnelling and Underground Space Technology*, vol. 81, pp. 83–93, 2018.

[26] Z. Y. Chen, G. S. Su, J. W. Ju, and J. Q. Jiang, "Experimental study on energy dissipation of fragments during rockburst," *Bulletin of Engineering Geology and the Environment*, vol. 78, no. 7, pp. 5369–5386, 2019.

[27] N. Li, Y. S. Zou, S. C. Zhang et al., "Rock brittleness evaluation based on energy dissipation under triaxial compression," *Journal of Petroleum Science and Engineering*, vol. 183, Article ID 106349, 2019.

[28] F. Wang and R. Kaunda, "Assessment of rockburst hazard by quantifying the consequence with plastic strain work and released energy in numerical models," *International Journal of Mining Science and Technology*, vol. 29, no. 1, pp. 93–97, 2019.

[29] P. Ying, Z. M. Zhu, F. Wang, M. Wang, C. Y. Niu, and L. Zhou, "The characteristics of dynamic fracture toughness and energy release rate of rock under impact," *Measurement*, vol. 147, Article ID 106884, 2019.

[30] X. C. Hu, G. S. Su, G. Y. Chen et al., "Experiment on rockburst process of borehole and its acoustic emission characteristics," *Rock Mechanics and Rock Engineering*, vol. 52, no. 3, pp. 783–802, 2019.

[31] G. S. Su, Y. J. Shi, X. T. Feng, J. Q. Jiang, J. Zhang, and Q. Jiang, "True-triaxial experimental study of the evolutionary features of the acoustic emissions and sounds of rockburst processes," *Rock Mechanics and Rock Engineering*, vol. 51, no. 2, pp. 375–389, 2018.

[32] X. M. Sun, H. C. Xu, L. G. Zheng, M. C. He, and W. L. Gong, "An experimental investigation on acoustic emission characteristics of sandstone rockburst with different moisture contents," *Science China Technological Sciences*, vol. 59, no. 10, pp. 1549–1558, 2016.